MARS ATMOSPHERIC THERMAL STRUCTURE DURING THE 1ST YEAR OF TGO SOLAR OCCULTATION MEASUREMENTS.

Miguel Angel López-Valverde, *(valverde@iaa.es)*, **B. Funke, A. Brines, A. Modak, A. Stolzenbach, F. González-Galindo, B. Hill, J. J. López-Moreno,** *Instituto de Astrofísica de Andalucia (IAA/CSIC), Granada, Spain (valverde@iaa.es)*, **I. Thomas, L. Trompet, J. Erwin,** *Belgian Royal Institute for Space Aeronomy, Brussels, Belgium*, **S. Aoki,** *University of Tokyo, Japan*, **Gerónimo Villanueva,** *NASA Goddard Space Flight Center, USA*, **Giuliano Liuzzi,** *American University, Washington DC, USA*, **F. Forget,** *Laboratoire de Meteorologie Dynamique, Paris, France*, **Giancarlo Bellucci,** *Institute for Space Astrophysics and Planetology, Italy*, **Manish Patel,** *Open University, Milton Keynes, UK*, **Bojan Ristic, Frank Daerden, Ann-Carine Vandaele,** *Belgian Royal Institute for Space Aeronomy, Brussels, Belgium*.

Introduction

The detailed variation of temperature and density with altitude is of paramount importance to characterize the atmospheric state and to constrain the chemistry, radiation and dynamics as a whole. Only with an accurate description of vertical variations with the best possible spatial and resolution we can aim at describing the key exchanges between atmospheric layers. These are needed for transport of radiatively active species, for energy budget modeling, including photochemistry, gravity wave propagation and global dynamics, and for atmospheric escape processes, to mention a few.

The power of solar occultation The NOMAD and the Atmospheric Chemistry Suite (ACS) are the two key instruments for atmospheric research on board the ExoMars 2016 Trace Gas Orbiter, primarily devoted to trace gas detection and mapping [15, 4]. The solar occultation observational strategy of these two instruments offers a unique opportunity to sound also up to high altitudes with an unprecedented vertical resolution in order to perform unprecedented sounding at mesospheric and thermospheric altitudes [6].

Goals This is the long term target of our team, and in this work we present first results. We analyzed transmittance spectra obtained from the NOMAD solar occultation channel, with a state-of-the-art retrieval scheme, adapted from Earth to Mars conditions and geometry, to derive temperature and density up to about 100 km. We will present the quality and robustness of the inversions and its application to the study of the variability of the Martian thermal structure in the troposphere and mesosphere during the 1st first year of the TGO science phase, from April 2018 to March 2019, which covers approximately two Mars seasons. These range from solar longitudes Ls 160° to Ls 360°, i.e., the Southern spring and summer seasons, sometimes collectively named as the Martian perihelion period.
The results presented here follow upon a recent work submitted to a special issue devoted to the analysis of the first year of TGO observations [7].

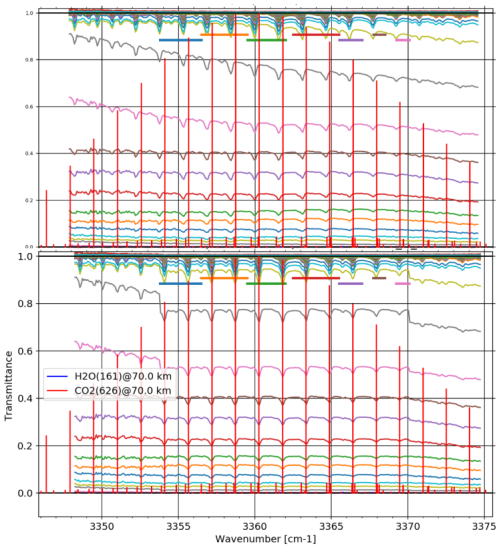

Figure 1: Example of our cleaning method applied to diffraction order 149 in one specific scan (20180423_204351_1p0a_SO_A_I). Top panel, all the original calibrated transmittance spectra taken in this scan, each tangent altitude with a different color, showing clear bending effects and spectral shifts. Bottom panel, the same spectra after cleaning, which is only applied to a subset of the full diffraction order on purpose. Vertical red solid lines indicate the CO_2 spectral lines positions (Hitran2016).

Datasets

The NOMAD spectrograph operationally measures the atmospheric absorption in several diffraction orders. The data analyzed here are calibrated transmittances in the so called order 149, containing moderately strong CO_2 lines. The nominal measurement uncertainties seem to contain small but clear systematics which are under investigation. We use here an estimation of their random component, as a first approach. Other effects which are corrected for during a "pre-processing phase" of our data analysis include spectral shifts and a residual spec-

tral bending across each diffraction order, which vary significantly from scan to scan, as they depend on temperature effects on the detector, on TGO orbital conditions which in turn impact the space signals, and on drifts through time in the behavior of the grating's blaze response [5, 13]. These effects and their correction are shown for one specific scan in Figure 1.

Let us note in particular the importance of a correct handling of the "bending" mentioned above for a proper description of the baseline continuum, specially at high altitudes, where a deficient correction may introduce biases larger than the actual absorption lines. The bending spectral shape can approximately be characterized by a polynomial function but its precise removal requires to take into account the gas absorption lines, i.e., a detailed line-by-line forward model calculation.

Retrieval Scheme

Our retrieval scheme is based on a state-of-the-art line-by-line forward model called KOPRA ([12]) and an inversion control program (RCP, [16]) well tested in Earth remote sounding experiments. RCP performs a global fit of 1-D vertical profiles of radiance spectra, assuming homogeneity in the horizontal along the line-of-sight. RCP solves iteratively the inverse problem (Rodgers, 2000) until convergence is achieved. The calculation of the model spectra and Jacobians is performed with KOPRA, in each step of the iteration, including a hydrostatic adjustment in each iteration, to account for the varying atmospheric state when the thermal structure is changed, and therefore to guarantee realistic results in the temperature/pressure structure. The hydrostatic adjustment assumes a reference pressure at the lowermost tangent altitude available, and this value is taken from the *a priori* reference atmosphere. The *a priori* temperature and density profiles are taken from a specific run of the Mars Global Climate Model developed at the Laboratoire de Météorologie Dynamique (LMD-MGCM) [2], using the recent implementations of the water cycles [10] and the dust scenarios appropriate for MY34 [8].

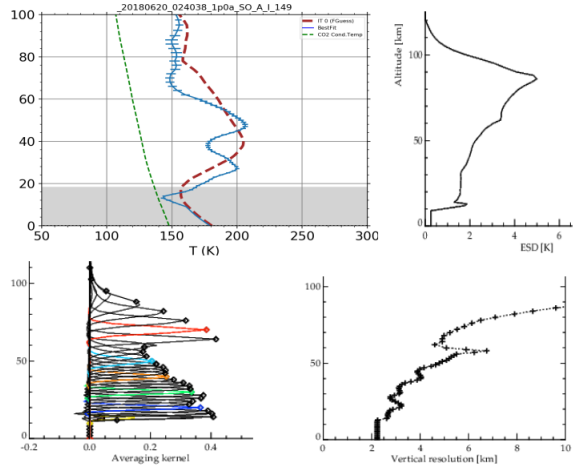

Figure 2: Retrieved temperature profile from scan *20180423_204351_1p0a_SO_A_I* with error bars (top-left panel), where the red dashed line is the *a priori* profiles, and the green dashed line is the CO_2 condensation temperature, added for reference. Bottom-left: rows of the Averaging Kernel matrix selected at some altitudes. Top-right: retrieval error in the Temperature profile. Bottom-right: Vertical resolution, as given by the widths of the averaging kernel rows.

Figure 2 shows the performance of the temperature inversion in one specific scan obtained on June 20th, 2018, for Ls 196° and at 55° N latitude, where a heavy dust loading was found below about 20 km. In addition to the noise propagation, the vertical resolution, as given by the width of the Averaging Kernels rows, is essential for comparing results to other retrievals and to models. With our optimal regularization, the vertical resolution varies with the tangent altitude, between 3 km and 9 km, and typical retrieval errors vary between 1.5-3.5 K.

Retrieved atmospheric temperatures

We describe the over 330 retrieved profiles during MY34 in detail in [7]. Here we highlight a few results which will be discussed in the Workshop.

Figure 3 shows all the temperature profiles retrieved in this work, put together in a single panel, with a similar plot for the LMD GCM profiles (our *a priori*). The dashed lines in blue and orange represent the envelope of all possible temperatures anywhere and anytime on Mars, taken from [11], who compiled data from instruments Mars Climate Sounder and Thermal Emission Spectrometer, as well as from the Mars Climate Database simulations for extreme conditions. An overall agreement exists in the lower atmosphere but at mesospheric altitude the NOMAD temperatures are globally colder than in the GCM by about 10 K.

The atmospheric thermal structure during the two Mars seasons in MY34 (the Martian perihelion half-year period) and shown in Figure 4 is characterized by the strong MY34 global dust storm (GDS) episode, a well documented event peaking around Ls 195°-210° [3, 8]. Our results show that the GDS warmed the atmosphere significantly at all altitudes, with episodes where 180 K are observed at 80 km altitude in the NH and up to 100 km in the SH. The thermal impact is clearly observed during an extended decay phase up to about Ls 250°. The impact of a smaller scale "regional" dust storm which occurred around Ls 320°, near the end of the period studied in this work, is less clear in our data, perhaps due to inadequate sampling.

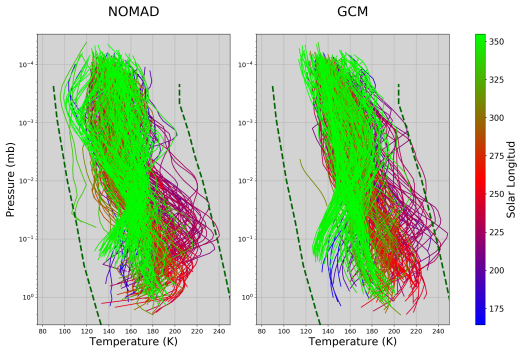

Figure 3: Envelope of all the retrieved temperature profiles (left-hand panel) compared to the *a priori* data, from the LMD-MGCM (right-hand panel). The colors in each scan indicate the Solar Longitude. The thick dashed lines represent the extreme temperatures at any time and place on Mars, after [11].

Atmospheric densities

Figure 5 shows the global distribution of all the CO_2 densities obtained at an altitude of 70 km, together with the GCM variability at that altitude. There are clear variations associated with the latitudinal change at the tangent point. In both hemispheres the sign of the response is similar: as the orbit approaches lower latitudes the density increases, following the warmer troposphere at low latitudes. Averaging over these variations one can discern a seasonal trend with a maximum around the summer in the SH, around Ls 270°, when the atmospheric density in Mars presents a maximum. However, in Figure 5 the maximum is observed around Ls 200°, as a response to the MY34 GDS.

This analysis is complementary and agrees with a similar study of density variability using NOMAD data

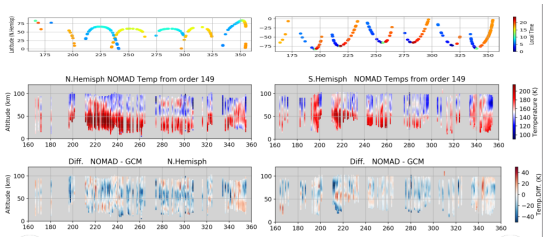

Figure 4: Distribution of all the retrieved temperatures with latitude and solar time throughout MY34, split in the two hemispheres (NH in the left hand side panels and SH in the right hand side panels). The top panels show the latitudes and the Local Solar Time of the observations. The center panels show the temperatures, and the lower panels the difference between the NOMAD retrievals and the GCM (*a priori*).

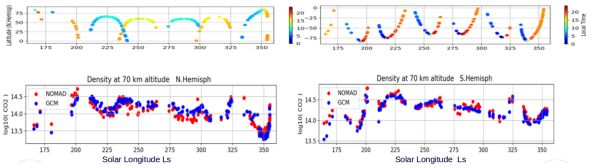

Figure 5: Global distribution of the retrieved CO_2 densities for MY34, split in the two hemispheres (NH in panels on the left and SH on the right). The top panels show the latitudes and the Local Solar Time of the observations and the central panels show the densities in log scale. The bottom panels show the density variation at 70 km altitude through the mission, including latitudinal and seasonal variations (see text); red dots: NOMAD densities, blue dots: GCM data.

by [14], using another diffraction order, targeting a different observational period (MY35 and MY36, excluding MY34) and focused on mesospheric altitudes. Although devoted to a non-GDS year, their density absolute values at 70 km agree well between with our results for MY34.

Local time variability This type of studies is possible using solar occultation data if one takes care of excluding very high latitudes and search for proper times during the TGO mapping. Here we grouped the results for latitudes 30°N-60°N and for solar Longitude Ls 290°-310° and examined their changes with the local time. Figure 6 shows the differences between morning and evening data, including the LMD GCM profiles for the same scans. The NOMAD profiles are more wavy than in the model, with a possibly upward propagating wave with large amplitudes, around 30 K in the mesosphere, which is much weaker in the GCM. The warm layer at 80 km in the NOMAD morning data could be related to the recent finding of a warm layer at precisely that altitude at nighttime in stellar occultation data from IUVS/Maven [9].

A similar warm layer was reported also by [1] using ACS solar occultation data in the ACS/MIR channel. These data are not exactly collocated with NOMAD observations, but combined with our results, we claim that there seems to be a peculiar period of time around

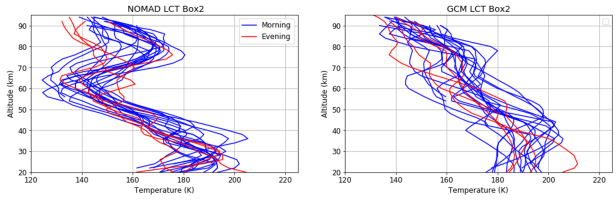

Figure 6: Local Time variations in a location box defined Latitudes 30°N-60°°N and Ls 290°-310°, to minimize latitudinal and seasonal effects. Blue and read lines are morning and evening data, respectively.

perihelion, at the end of the Southern summer where thermal tides at mid latitudes seem to present very strong amplitudes, greatly affecting the lower mesosphere.

Acknowledgments

The IAA/CSIC team acknowledges financial support from the State Agency for Research of the Spanish MCI through the 'Center of Excellence Severe Ochoa' award (DEV-2017-0709) and funding by grant PGC2018-101836-B-100 (MCI/AEI/FEDER, EU). FGG is funded by the project RTI2018-100920-J-I00 (MCI/AEI/FEDER, EU). This project acknowledges funding by the Belgian Science Policy Office (BELLS), with the financial and contractual coordination by the ESAU Prod ex Office (PEA 4000103401, 4000121493) as well as by UK Space Agency through grants ST/V002295/1, ST/V005332/1 and ST/S00145X/1 and Italian Space Agency through grant 2018-2-HHS.0. US investigators were supported by the National Aeronautics and Space Administration.

References

[1] D. A. Belyaev et al. Revealing a high water abundance in the upper mesosphere of mars with acs onboard tgo. *Geophysical Research Letters*, 48(10):e2021GL093411, 2021. e2021GL093411 2021GL093411.

[2] F. Forget et al. Improved general circulation models of the Martian atmosphere from the surface to above 80 km. *J. Geophys. Res.*, 104:24,155–24,176, 1999.

[3] S. D. Guzewich et al. Mars science laboratory observations of the 2018/mars year 34 global dust storm. *Geophysical Research Letters*, 46(1):71–79, 2019.

[4] O. Korablev et al. The atmospheric chemistry suite (acs) of three spectrometers for the exomars 2016 trace gas orbiter. *Space Sci. Rev*, 214(1):62, Feb 2018.

[5] G. Liuzzi et al. Methane on mars: New insights into the sensitivity of ch4 with the nomad/exomars spectrometer through its first in-flight calibration. *Icarus*, 321, 09 2018.

[6] M. A. López-Valverde and others. Investigations of the mars upper atmosphere with exomars trace gas orbiter. *Space Science Reviews*, 214(1):29, Jan 2018. Como citar este articulo: López-Valverde, M.A., Gerard, JC., González-Galindo, F. et al. Space Sci Rev (2018) 214: 29. https://doi.org/10.1007/s11214-017-0463-4.

[7] M. A. López-Valverde et al. Martian atmospheric temperature and density profiles during the 1st year of nomad/tgo solar occultation measurements. *JGR-Planets, submitted*, 2022.

[8] L. Montabone et al. Martian year 34 column dust climatology from mars climate sounder observations: Reconstructed maps and model simulations. *Journal of Geophysical Research: Planets*, 125(8):e2019JE006111, 2020.

[9] H. Nakagawa et al. A warm layer in the nightside mesosphere of mars. *Geophysical Research Letters*, 47(4):e2019GL085646, 2020. e2019GL085646 2019GL085646.

[10] T. Navarro et al. Detection of detached dust layers in the martian atmosphere from their thermal signature using assimilation. *Geophysical Research Letters*, 41(19):6620–6626, 2014.

[11] M. D. Smith et al. *Thermal Structure and Composition*, chapter 4, pages 42–75. Cambridge Planetary Science. Cambridge University Press, 2017.

[12] G. P. Stiller, editor. *The Karlsruhe Optimized and Precise Radiative Transfer Algorithm (KOPRA)*, volume FZKA 6487 of *Wissenschaftliche Berichte*. Forschungszentrum Karlsruhe, 2000.

[13] I. R. Thomas et al. Calibration of nomad on esa's exomars trace gas orbiter: Part 1 ? the solar occultation channel. *Planetary and Space Science*, page 105411, 2021.

[14] L. Trompet et al. Carbon dioxide retrievals from nomad-so on esa?s exomars trace gas orbiter and temperature profiles retrievals with the hydrostatic equilibrium equation. i. description of the method. *JGR-submitted*, 2022.

[15] A. C. Vandaele et al. Nomad, an integrated suite of three spectrometers for the exomars trace gas mission: Technical description, science objectives and expected performance. *Space Science Reviews*, 214(5):80, 6 2018.

[16] T. von Clarmann et al. Retrieval of temperature and tangent altitude pointing from limb emission spectra recorded from space by the Michelson Interferometer for Passive Atmospheric Sounding (MIPAS). *J. Geophys. Res.*, 108(D23), 2003.